Reduced Graphene Oxide-Wrapped Super Dense Fe₃O₄ Nanoparticles with Enhanced Electromagnetic Wave Absorption Properties

Qi Yu [1],*, Yiyi Wang [1], Ping Chen [2],*, Weicheng Nie [1], Hanlin Chen [1] and Jun Zhou [1]

[1] Faculty of Materials Science and Engineering & Liaoning Key Laboratory of Advanced Polymer Matrix Composites, Shenyang Aerospace University, Shenyang 110136, China; w13516017108@126.com (Y.W.); nie0301@126.com (W.N.); q13019399662@163.com (H.C.); toutes@163.com (J.Z.)

[2] School of Chemical Engineering & State Key Laboratory of Fine Chemicals, Dalian University of Technology, Dalian 116024, China

* Correspondence: yuqi@sau.edu.cn (Q.Y.); pchen@dlut.edu.cn (P.C.);
Tel.: +86-024-89723970 (Q.Y.); +86-0411-84986100 (P.C.)

check for updates

Abstract: The efficient preparation of electromagnetic wave absorbing materials with low density and excellent electromagnetic wave absorption remains a considerable challenge. In this study, reduced graphene oxide (RGO) wrapped Fe₃O₄ nanoparticles (NPs) were synthesized based on one-step reaction by the reduction of graphene oxide (GO), and the generation of super-fine Fe₃O₄ NPs was achieved. The phase structure, chemical composition, micromorphology, and magnetism were characterized by X-ray diffraction (XRD), X-ray photoelectron spectroscope (XPS), scanning electron microscope (SEM), transmission electron microscope (TEM), and vibrating sample magnetometer (VSM), respectively. The electromagnetic characteristics were evaluated on a vector network analyzer by the coaxial line method. The results showed that super-fine Fe₃O₄ NPs with an average size of 6.18 nm are densely distributed on the surface of graphenes. The RGO/Fe₃O₄ nanocomposites exhibited excellent microwave absorption properties with a minimum reflection loss (RL) of up to −55.71 dB at 6.78 GHz at 3.5 mm thickness and the highest effective absorption bandwidth with RL values exceeding −10 dB is 4.76 GHz between 13.24 and 18 GHz at 1.7 mm thickness. This work provides a concise method for the development of RGO supported super dense Fe₃O₄ nanocomposites for high performance electromagnetic absorption applications.

Keywords: RGO/Fe₃O₄ nanocomposite; micromorphology; electromagnetic characteristics; microwave absorption properties

1. Introduction

Due to the rapid development of electromagnetic wave detection technology, high performance microwave absorption materials have attracted more and more attention in the civil and military industries [1–3]. Ferrites have been widely used as electromagnetic wave (EW) absorbing agents due to their high saturation magnetization, low technological threshold, and cost [4,5]. Unfortunately, traditional ferrite absorbers have revealed shortcomings such as easy aggregation, high weight, and an inefficient EW absorption capability in practical applications. In general, these shortcomings are confined to the effects of magnetic loss when attenuating EW signals for Fe₃O₄ nanoparticles (NPs) due to their high resistivity, but a single loss mechanism is not beneficial for the achievement of ideal EW absorption performance. Thus, it is necessary to introduce some other types of electromagnetic loss mechanisms to alleviate this dilemma [6–8].

Recently, graphene nanosheets (GNs) have gained a lot of attention as microwave absorbers by virtue of their excellent conductivity and light weight [9–11]. Researchers have found that reduced graphene oxide (RGO) has attractive microwave absorbing ability owning to its high dielectric loss. Nevertheless, single RGOs could not achieve ideal microwave absorption performance due to their high permittivity and low permeability, which would lead to unfavorable electromagnetic impedance matching. In order to mitigate the dilemma, a lot of research has been conducted by combining RGO with magnetic components, such as FeCo [12], Ni [13], NiCoP [14], $CoFe_2O_4$ [15], and Fe_3O_4 [16]. For example, Xu et al. synthesized RGO/Ni hybrids with different mass ratios to obtain an optimal reflection loss value of −39.03 dB at 13 GHz [13]. Xue et al. synthesized NiCoP/RGO nanocomposites by one-pot reaction in order to improve dielectric and magnetic loss and thus enhance the reflection loss [14]. Chu et al. synthesized α-Fe_2O_3/RGO with a maximum reflection loss of up to −42.8 dB at a thickness of 1.8 mm [16]. Therefore, decorating magnetic metal NPs onto the large surface of GNs is a flexible strategy for improving microwave absorption properties by combining dielectric and magnetic loss mechanisms into a micro-nano composite structure, which can also improve their aggregation resistance and reduce their weight [17–26].

Herein, we report an easy and efficient method for the synthesis of graphene wrapped super dense Fe_3O_4 NPs via one-step reaction in order to enhance their microwave absorption properties. The phase structure, chemical composition, micromorphology, and magnetism of RGO/Fe_3O_4 nanocomposites are investigated, and the electromagnetic parameters and microwave absorption performance of RGO/Fe_3O_4 is evaluated.

2. Materials and Methods

All chemical reagents including ferric chloride ($FeCl_3$), diethylene glycol (DEG), potassium permanganate ($KMnO_4$), hydrogen peroxide (H_2O_2), concentrated sulfuric acid (H_2SO_4), and NaOH were purchased from Sinopharm Chemical Reagent Company (Shanghai, China). Graphite power was supplied by Yanhai Carbon Material Company (Qingdao, China).

Graphene oxide (GO) was synthesized using modified Hummers method [27]. The source materials (2 g of graphene powder, 60 mL of concentrated H_2SO_4, and 7 g of $KMnO_4$) were successively put into a three-necked flask while undergoing mechanical stirring in an ice water bath. The mixture was heated to 35 °C while undergoing mechanical stirring for 3 h, and then diluted with distilled water (100 mL) dropwise. Afterwards, the mixture was heated to 90 °C while undergoing strong mechanical stirring for 30 min. Finally, distilled water (180 mL) and H_2O_2 (20 mL, 30%) were added dropwise and then the mixture was kept undisturbed for 24 h. The obtained precipitation was washed with HCl solution and distilled water through centrifugation until the decantate became neutral. Finally, the resulting graphene oxides (GOs) were obtained by ultrasonic treatment in water followed by freeze-drying.

The as-obtained GOs were firstly dissolved in 70 mL DEG, and 400 mg $FeCl_3$ was added while the mixture was being stirred, then the suspension was heated to 220 °C while undergoing continuous stirring for 1 h with the protection of argon. Afterwards, NaOH solution was quickly poured into the suspension while undergoing stirring for another 0.5 h at 220 °C. Finally, the reaction system was cooled down to room temperature and the obtained RGO/Fe_3O_4 was separated and purified by centrifugation, washing, and drying. For comparison, pure Fe_3O_4 NPs was prepared using similar methods.

The chemical composition was characterized by X-ray photoelectron spectroscopy (XPS) performed on a Thermo ESCALAB 250 (Thermo Fisher Scientific Inc., Waltham, MA, USA) with Al-K$_\alpha$ radiation. The micromorphology was observed by transmission electron microscopy (TEM) conducted on a Tecna G2 F20 S-TWIN electron microscope (FEI Inc., Hillsborough, OR, USA) operated at 200 kV. The hysteresis loop was recorded on a SQUID-VSM vibrating sample magnetometer (Quantum Design Inc., San Diego, CA, USA). Electromagnetic parameters, including relative complex permittivity and permeability, were measured in the frequency range of 1–18 GHz using the coaxial line method on an AV3629D Vector Network Analyzer (CETI Co., Qingdao, China) by mixing the samples with paraffin

wax (weight ratio of 1:1) and pressing them into a standard cylindrical shape mold with an inner diameter of 3 mm, an outer diameter of 7 mm, and a thickness of 3 mm.

3. Results and Discussion

3.1. Chemical Composition and Morphology

The chemical composition of the RGO/Fe_3O_4 nanocomposite was identified by XPS as shown in Figure 1. Figure 1a shows the XPS full spectrum of RGO/Fe_3O_4. It can be observed that the peaks located at around 56, 285, 532, and 711.3 eV belong to Fe3p, C1s, O1s and Fe2p, respectively, which indicates that RGO/Fe_3O_4 consists of three major elements including C, O and Fe. In the Fe2p high resolution XPS spectra shown in Figure 1b, the peaks located at 711 and 723 eV are assigned to Fe 2p$_{3/2}$ and Fe 2p$_{1/2}$, respectively, which is consistent with the characteristic peaks of Fe_3O_4.
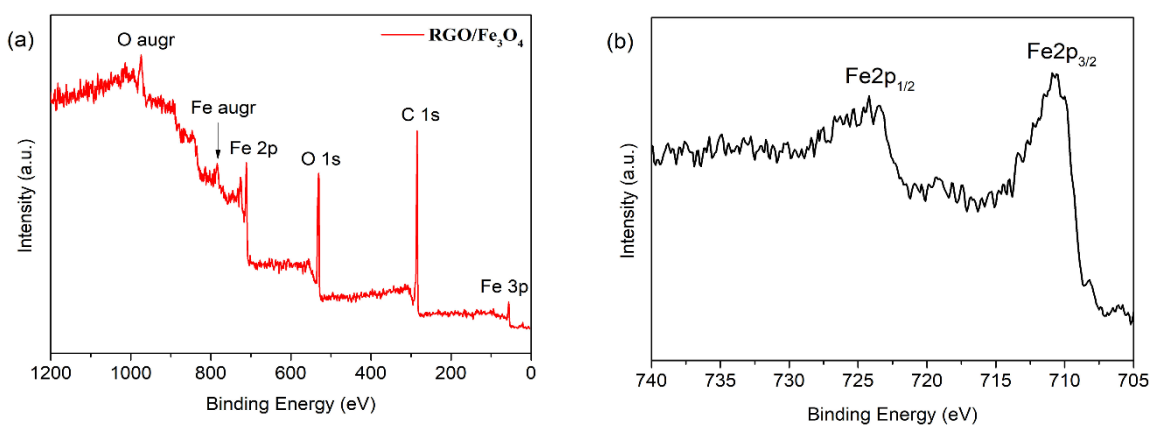

Figure 1. X-ray photoelectron spectroscope (XPS) spectra of reduced graphene oxide (RGO)/Fe_3O_4 nanocomposite: (**a**) full spectrum, (**b**) Fe2p high resolution spectrum.

Figure 2 shows transmission electron microscopy (TEM) images of RGO/Fe_3O_4 nanocomposite. It can be seen from Figure 2a,b that the wrinkled surface of graphene nanosheets, which are capable of supplying a large loading area for NP growth, are homogeneously decorated with super dense spherical Fe_3O_4 NPs. The tiny Fe_3O_4 NPs, with an average size of 6.18 nm, are well distributed on the surface of the graphenes. In the loading process, GOs were employed as a flexible substrate for the in situ anchoring of Fe^{3+} and its growth into Fe_3O_4 NPs, so they played a confinement function to prevent the Fe_3O_4 NPs from detaching and aggregating. In the HRTEM image shown in Figure 2c, the interplanar distance of the NPs is 0.25 nm, which is in accordance with the lattice spacing of the (311) plane of cubic magnetite Fe_3O_4, further confirming the formation of Fe_3O_4 nanocrystals on the surface of RGO inferred from the XPS results.
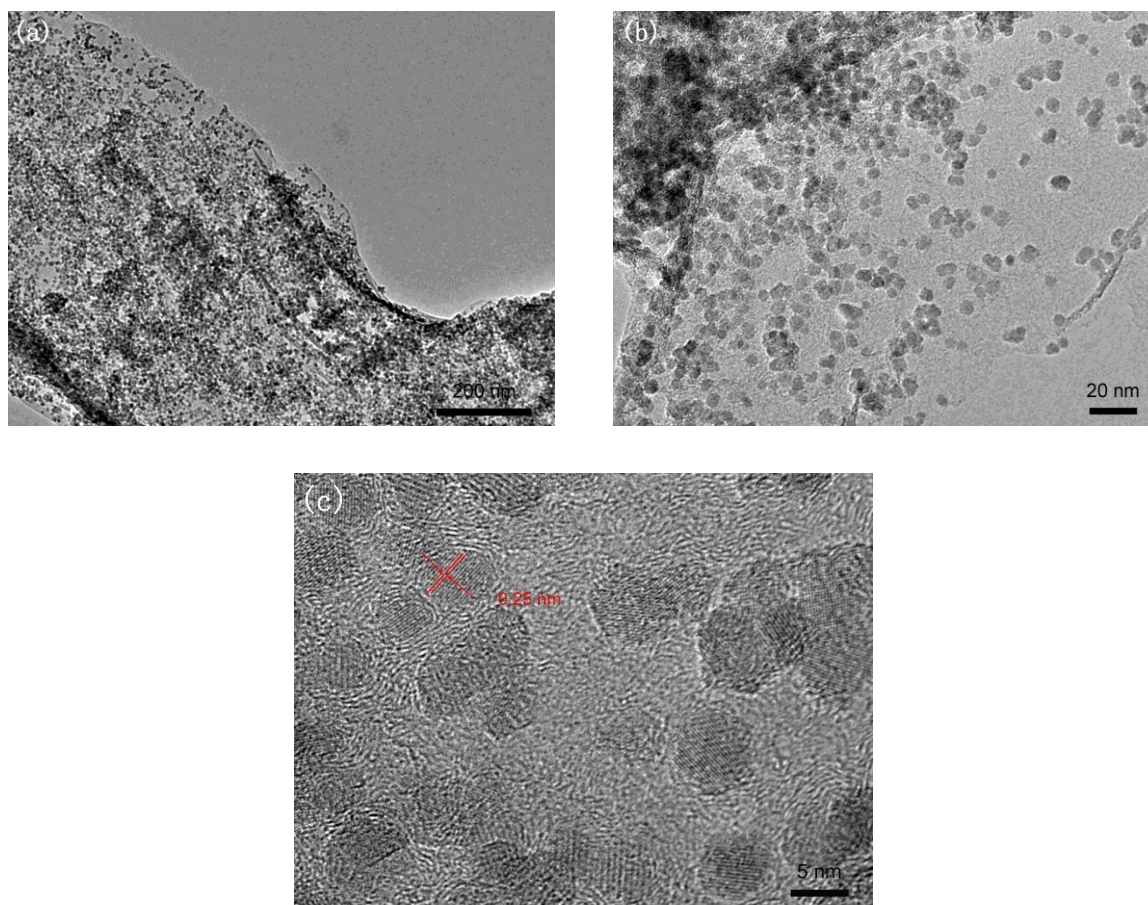
Figure 2. (**a**,**b**) TEM and (**c**) HRTEM images of RGO/Fe$_3$O$_4$ nanocomposite.

3.2. Magnetic Properties

Figure 3a shows the hysteresis loops of different samples collected by a magnetometer at room temperature. The saturation magnetization (Ms) value of the RGO/Fe$_3$O$_4$, RGO, and Fe$_3$O$_4$ NPs are 36, 0.06, and 59 emu/g, and the corresponding coercivity (Hc) values are 25, 0, and 25 Oe, respectively. It can be observed that the Ms values for Fe$_3$O$_4$ NPs are higher than those of RGO/Fe$_3$O$_4$ and RGOs, indicating that the magnetism of RGO/Fe$_3$O$_4$ is introduced by loading magnetic Fe$_3$O$_4$ NPs onto the surface of nonmagnetic RGOs. Meanwhile, the Hc values of RGO/Fe$_3$O$_4$ and Fe$_3$O$_4$ NPs are the same, suggesting that the loading process has no effect on the intrinsic magnetic properties of Fe$_3$O$_4$ NPs. To further illustrate the magnetic properties, the RGO/Fe$_3$O$_4$ were dispersed in an ethanol solution (Figure 3b), which has favorable dispersibility and stability. After being attracted by a magnet (Figure 3c), the RGO/Fe$_3$O$_4$ dispersed in alcohol were quickly gathered together and attached to the bottle wall. Therefore, the graphenes were successfully magnetized by the loading of super dense Fe$_3$O$_4$ NPs.
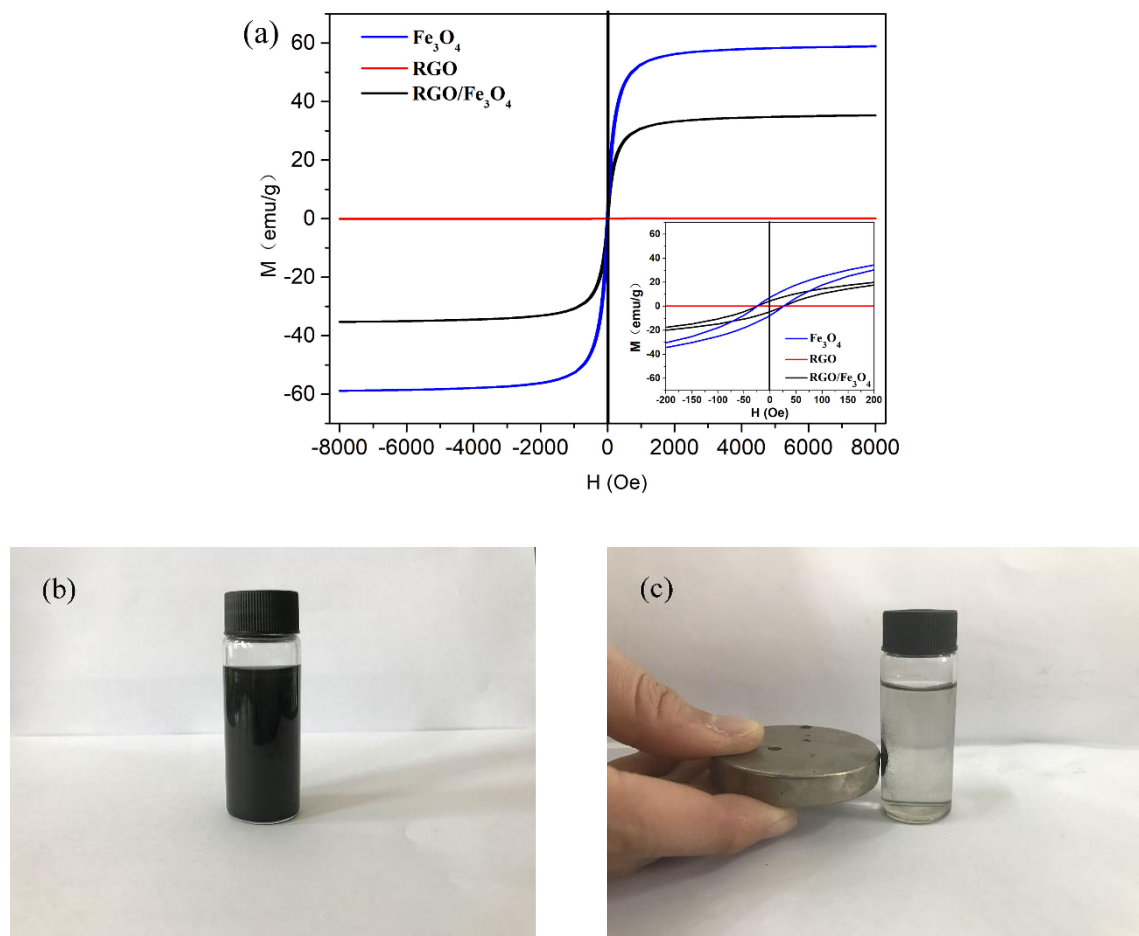
Figure 3. (**a**) Hysteresis loops of different samples measured at 298 K, (**b**) RGO/Fe$_3$O$_4$ nanocomposites dispersed in alcohol, and (**c**) separated by a magnet.

3.3. Electromagnetic Characteristics

In order to find out the essential reasons for microwave absorption mechanisms, the electromagnetic parameters, including the complex permittivity and permeability of Fe$_3$O$_4$ NPs, RGO, and RGO/Fe$_3$O$_4$ nanocomposites, were measured. The real parts (ε' and μ') symbolize the storage capacity of electric and magnetic energy, and the imaginary parts (ε'' and μ'') symbolize the energy loss, respectively. The dielectric loss ($tan\delta_\varepsilon = \varepsilon''/\varepsilon'$) and magnetic loss tangent ($tan\delta_\mu = \mu''/\mu'$) give the balance between the real and imaginary parts in an absorbing structure.

Figure 4a–c show the frequency dependence of the real part (ε') and the imaginary part (ε'') of complex permittivity, and the dielectric loss tangent ($tan\delta_\varepsilon$) for different samples. It is clear that the ε', ε'', and $tan\delta_\varepsilon$ values for both RGO/Fe$_3$O$_4$ and RGO are larger than those of Fe$_3$O$_4$ NPs. The ε' of RGO/Fe$_3$O$_4$ declines from 13.69 to 6.98 with increasing frequency, and the ε'' remains relatively stable, changing from 5.55 to 3.04. The $tan\delta_\varepsilon$ curve also exhibits a moderate growth trend ranging from 0.33 to 0.65 with some fluctuation, particularly in the high frequency region. Compared with pure RGOs, the RGO/Fe$_3$O$_4$ have a similar tendency in ε', but it is slightly lower in ε'' and $tan\delta_\varepsilon$. The enhanced ε', ε'', and $tan\delta_\varepsilon$ of RGO/Fe$_3$O$_4$ is attributed to multiple dielectric loss behaviors derived from dielectric RGOs and magnetic Fe$_3$O$_4$ NPs. Firstly, the RGOs with high electric conductivity can form conducting networks, which is in favor of dielectric loss, thereby playing a main role in the substantial increase in ε', ε'', and $tan\delta_\varepsilon$ values. From the ε'' versus ε' plot of the RGO/Fe$_3$O$_4$ (Figure 4d), it can be observed that there are multi-arcs for RGO/Fe$_3$O$_4$ and RGO, while there are no obvious arcs with increasing frequency for Fe$_3$O$_4$ NPs, indicating that debye dipolar relaxation is the main dielectric loss mechanism

for RGO based nanostructure. In addition, the introduction of Fe_3O_4 NPs would create defects on the RGO surface, which would act as polarization centers for increasing dielectric loss. Secondly, although the sole Fe_3O_4 NPs with ε'' and $tan\delta_\varepsilon$ approaching zero have hardly any dielectric loss, loading Fe_3O_4 NPs onto the surface of RGOs can introduce extra dielectric polarization behaviors. The interfacial polarization might be strengthened by a multi-interface between Fe_3O_4 NPs and graphenes, and the different electric potential between the two would induce charge accumulation at both ends, thus enhancing the space-charge polarization. The super-tiny Fe_3O_4 NPs have unsaturated bonds, which can serve as dipoles, thus the dipole polarization is enhanced [28]. The above mentioned polarization processes are beneficial for the improvement of dielectric loss and for the better dissipation of microwave energy.
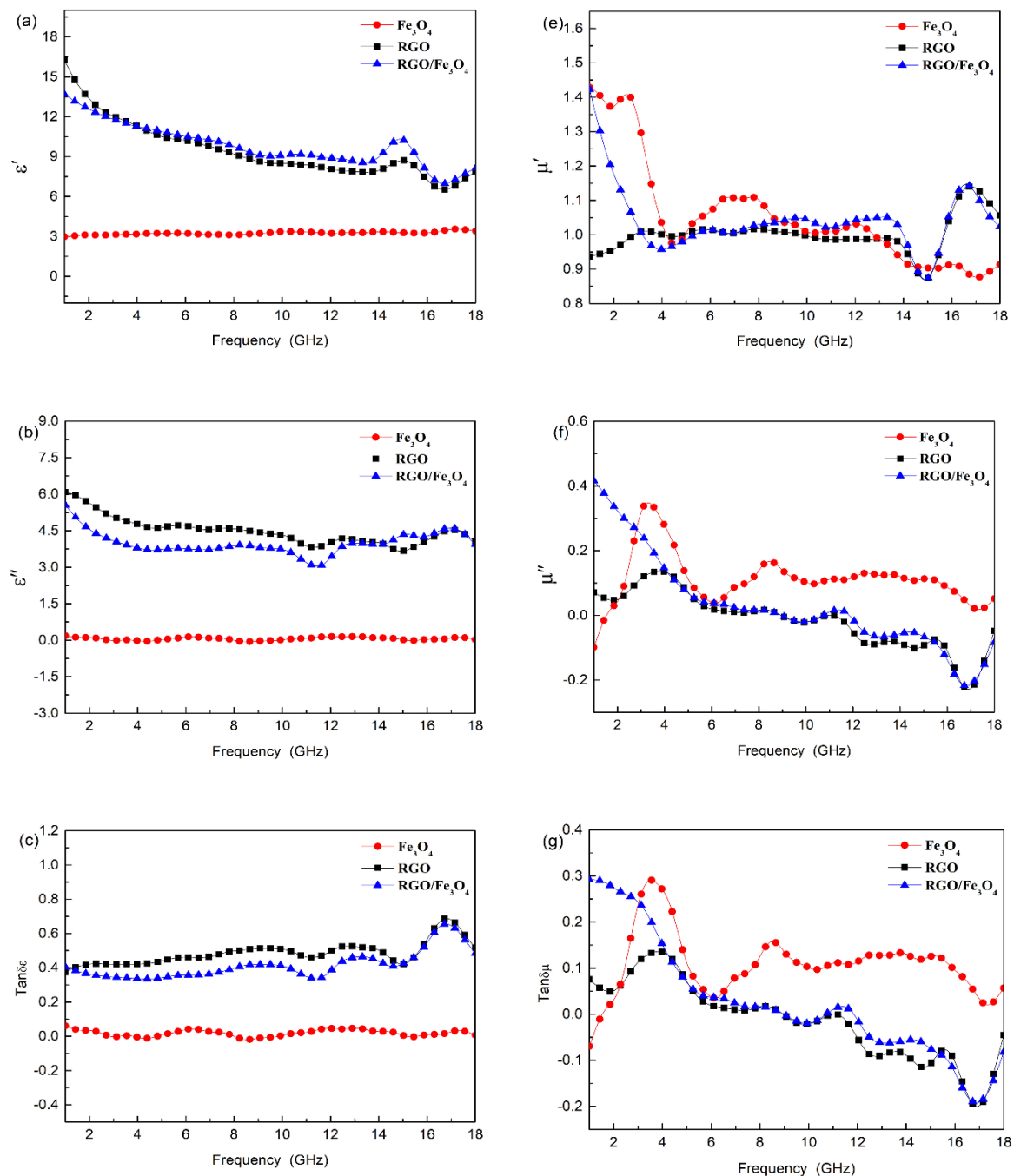

Figure 4. *Cont.*
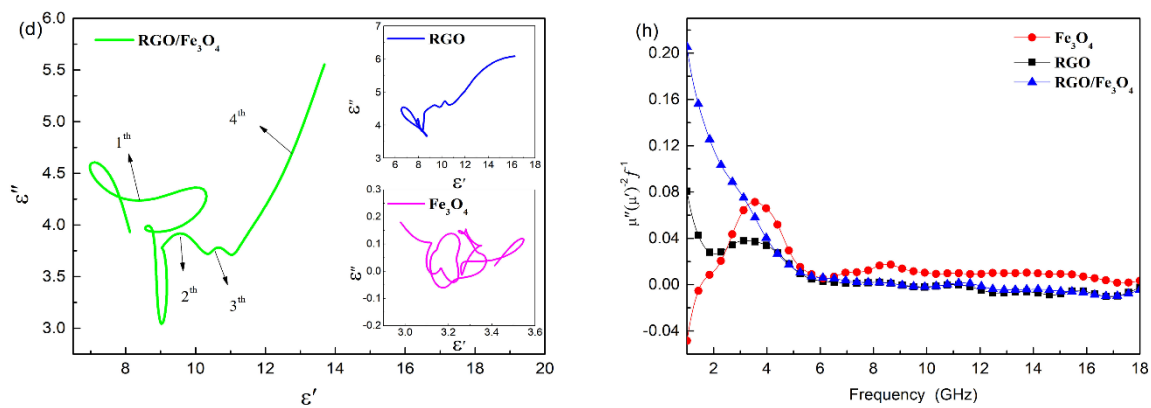
Figure 4. Electromagnetic characteristics of Fe_3O_4 nanoparticles (NPs), RGO and RGO/Fe_3O_4 nanocomposites: (**a**) real (ε') and (**b**) imaginary (ε'') parts of complex permittivity; (**c**) dielectric loss tangent ($tan\delta_\varepsilon$); (**d**) Cole–Cole semicircles (ε'' vs. ε'); (**e**) real (μ') and (**f**) imaginary (μ'') parts of complex permeability; (**g**) magnetic loss tangent ($tan\delta_\mu$); and (**h**) $\mu''(\mu')^{-2}f^{-1}$ vs. f.

Figure 4e–g show the real (μ') and imaginary (μ'') parts of the relative complex permeability, and the magnetic loss ($tan\delta_\mu$) for the different samples. It is seen that the μ' values for RGO/Fe_3O_4 and Fe_3O_4 NPs sharply decrease initially and then become relatively stabilized with some fluctuation as the frequency increases. The μ'' and $tan\delta_\mu$ for Fe_3O_4 NPs have obvious resonance peaks at 2–6 GHz, while there is a decreasing trend with increasing frequency in the μ'' and $tan\delta_\mu$ curve for RGO/Fe_3O_4, which are favorable for enhancing magnetic loss at low frequencies [29]. The multiple resonance peaks are mainly attributed to natural resonance derived from magnetic Fe_3O_4 NPs. When the spherical Fe_3O_4 NPs are smaller, the anisortropy constant is higher, and the natural resonance is stronger. Meanwhile, exchange resonance may also contribute to magnetic loss by a small amount and to the anisotropy of magnetic NPs. In addition, the $\mu''(\mu')^{-2}f^{-1}$ values have obvious fluctuations at 1–6 GHz but remain relatively stable subsequently (Figure 4h), indicating that the eddy-current loss may come into action after 6 GHz.

3.4. Microwave Absorption Properties

Figure 5 displays the changes in reflection loss (RL) versus frequency for the samples at different thicknesses. Figure 5a shows that the absorption performance of Fe_3O_4 NPs is so poor that the minimum RL is merely −4.41 dB at 13.07 GHz at a thickness of 3.3 mm. For RGO, shown in Figure 5b, the absorption performance gets better, with the minimum RL increasing to −26.87 dB at a thickness of 3.9 mm and shifting to a lower frequency of 4.31 GHz. It is implied from Figure 5c that the incorporation of RGOs can shift the minimum RL of Fe_3O_4 NPs to a lower frequency region with enhanced microwave absorption and an enlarged effective bandwidth. The reflection loss of RGO/Fe_3O_4 nanocomposites is greatly enhanced, with the minimum RL value reaching up to −55.71 dB at 6.78 GHz with a thickness of 3.5 mm, and the highest effective absorption bandwidth with RL values lower than −10 dB is 4.76 GHz between 13.24 and 18 GHz at a thickness of 1.7 mm (Figure 5d). For comparison, the microwave absorption properties of dielectric/magnetic nanocomposites studied in similar works are displayed in Table 1.
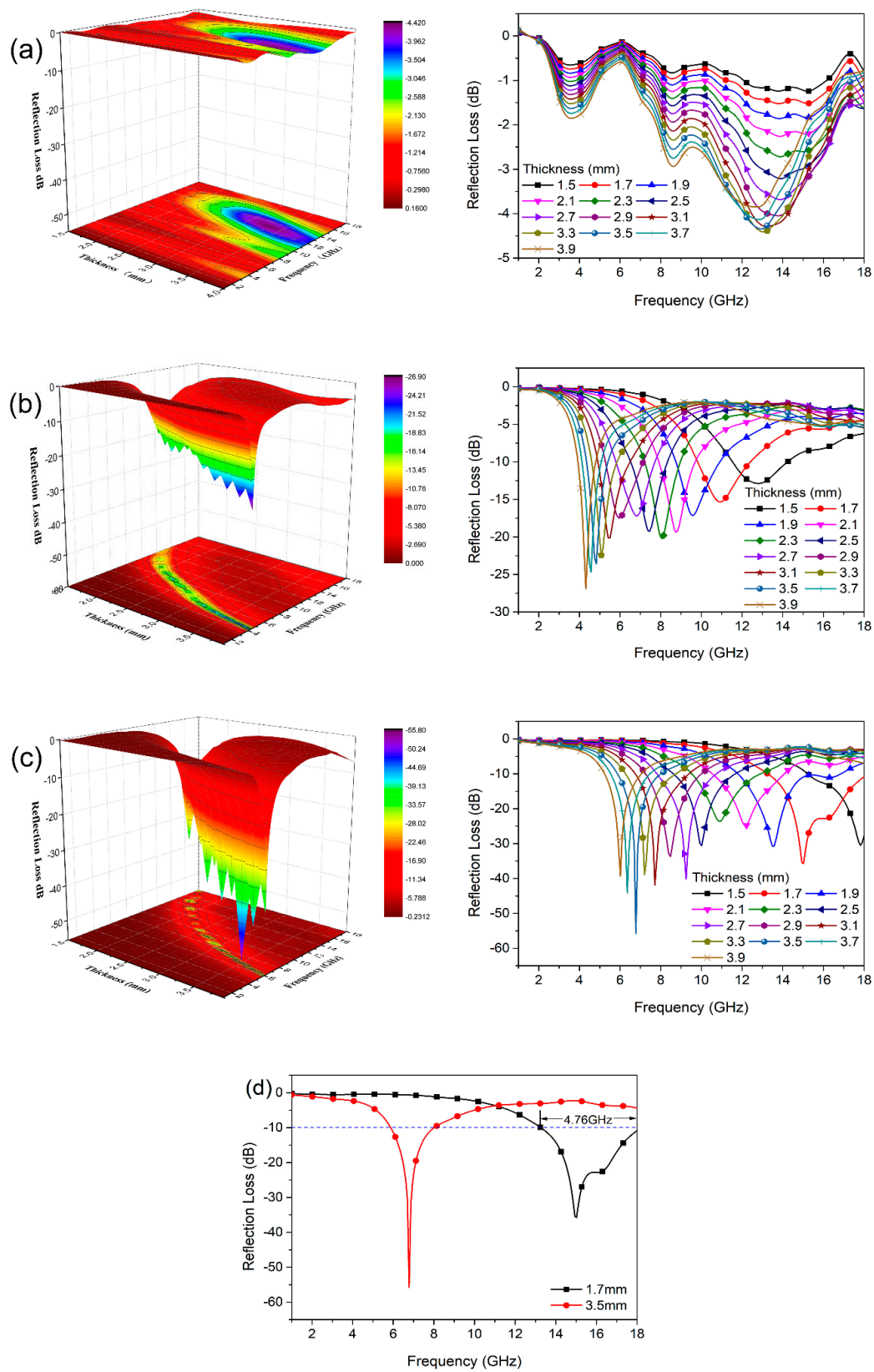
Figure 5. Reflection loss (RL) curves and 3D representation of (**a**) Fe_3O_4 NPs, (**b**) RGO, and (**c**) RGO/Fe_3O_4 with different thicknesses. (**d**) The RGO/Fe_3O_4 sample achieves an effective absorption bandwidth of 4.76 GHz at a thickness of 1.7 mm and reaches the maximum RL value of −55.71 dB (6.78 GHz) at a thickness of 3.5 mm.

Based on the above analysis, the enhanced microwave absorption properties of RGO/Fe$_3$O$_4$ nanocomposite can be attributed to multiple dielectric and magnetic loss mechanisms illustrated in Figure 6. The multi-interface introduced by super dense Fe$_3$O$_4$ NPs brought about extra polarization behaviors and magnetic loss, such as interfacial polarization, dipole polarization, space-charge polarization, eddy current loss, debye dipolar relaxation, natural resonance, and exchange resonance. All these processes improve the microwave absorption properties.

Table 1. Comparison of microwave absorption properties in this work and other representative works.

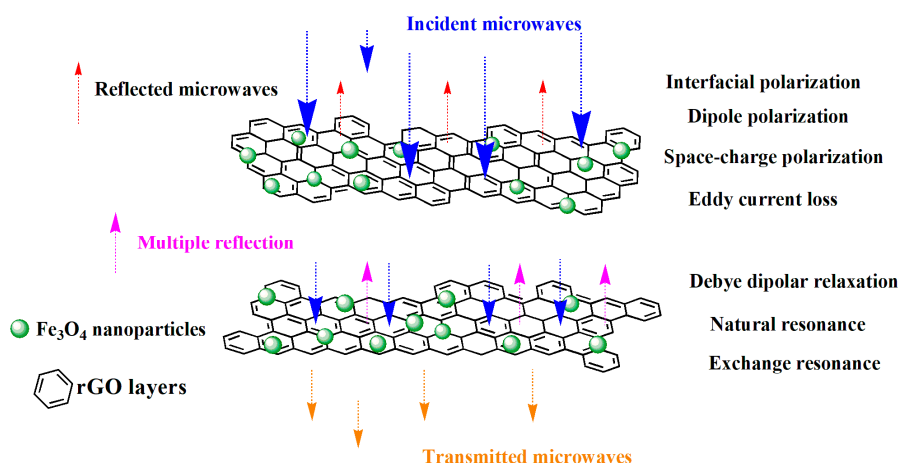| Absorber	Loading Ratio (wt%)	RL$_{min}$ (dB)	Effective Bandwidth (GHz) (RL < −10dB)	Thickness (mm)	Refs
RGO/Ni	50	−39.03	4.3	2.0	[13]
RGO/NiCoP	50	−17.84	3.5	1.5	[14]
Fe$_3$O$_4$/GO/CNT	30	−37.3	2.2	5	[30]
G/BaFe$_{12}$O$_{19}$/CoFe$_2$O$_4$	50	−32.4	3.0		[31]
Fe$_3$O$_4$/CNT	50	−20.1	1.4	3.5	[32]
RGO/CoFe$_2$O$_4$	60	−39.0	4.7	2.0	[15]
RGO/matrimony vine-like Fe$_3$O$_4$	50	−42.8	4.6	1.8	[22]
RGO/Fe$_3$O$_4$	50	−55.71	4.76	1.7	This work

Figure 6. Diagram of microwave absorbing mechanisms for RGO/Fe$_3$O$_4$ nanocomposite.

4. Conclusions

In summary, we have successfully synthesized RGO wrapped super dense Fe$_3$O$_4$ NPs via one-step reaction. The magnetic Fe$_3$O$_4$ NPs with an average size of 6.18 nm are well distributed on the surface of the graphenes. The RGO/Fe$_3$O$_4$ nanocomposites have shown excellent electromagnetic wave absorption properties. The minimum RL reaches up to −55.71 dB at 6.78 GHz at 3.5 mm thickness. The highest effective absorption bandwidth is 4.76 GHz between 13.24 and 18 GHz at 1.7 mm thickness. The multi-interface introduced by super dense Fe$_3$O$_4$ NPs brought about extra polarization behaviors and magnetic loss, both of which improved the microwave absorption properties. This work provides a concise way to develop graphene supported super dense Fe$_3$O$_4$ nanocomposites for high performance electromagnetic absorption applications.

Author Contributions: Conceptualization, Q.Y.; methodology, Q.Y.; validation, Q.Y. and P.C.; formal analysis, Y.W., H.C. and W.N.; investigation, Y.W. and H.C.; resources, Q.Y. and P.C.; data curation, W.N. and J.Z.; writing—original draft preparation, Q.Y.; writing—review and editing, Q.Y. and P.C.; visualization, Y.W.; supervision, P.C.; project administration, Q.Y.; funding acquisition, Q.Y. and P.C.

Conflicts of Interest: There are no conflicts of interest to declare.

References

1. Jian, X.; Wu, B.; Wei, Y.; Dou, S.; Wang, X.; He, W.; Mahmood, N. Facile Synthesis of Fe_3O_4/GCs Composites and their Enhanced Microwave Absorption Properties. *ACS Appl. Mater. Interfaces* **2016**, *8*, 6101–6109. [CrossRef] [PubMed]

2. Ren, F.; Zhu, G.; Ren, P.; Wang, K.; Cui, X.; Yan, X. Cyanate ester resin filled with graphene nanosheets and $CoFe_2O_4$-reduced graphene oxide nanohybrids as a microwave absorber. *Appl. Surf. Sci.* **2015**, *351*, 40–47. [CrossRef]

3. Xu, H.; Yin, X.; Zhu, M.; Han, M.; Hou, Z.; Li, X.; Zhang, L.; Cheng, L. Carbon Hollow Microspheres with a Designable Mesoporous Shell for High-Performance Electromagnetic Wave Absorption. *ACS Appl. Mater. Interfaces* **2017**, *9*, 6332–6341. [CrossRef] [PubMed]

4. Wang, Z.J.; Wu, L.N.; Zhou, J.G.; Shen, B.Z.; Jiang, Z.H. Enhanced microwave absorption of Fe_3O_4 nanocrystals after heterogeneously growing with ZnO nanoshell. *Rsc Adv.* **2013**, *3*, 3309–3315. [CrossRef]

5. Li, C.-J.; Wang, B.; Wang, J.-N. Magnetic and Microwave Absorbing Properties of Electrospun $Ba_{(1-x)}La_xFe_{12}O_{19}$ Nanofibers. *J. Magn. Magn. Mater.* **2012**, *324*, 1305–1311. [CrossRef]

6. Liu, Q.H.; Cao, Q.; Bi, H.; Liang, C.Y.; Yuan, K.P.; She, W.; Yang, Y.J.; Che, R.C. $CoNi@SiO_2@TiO_2$ and $CoNi@Air@TiO_2$ microspheres with strong wide-band micro-wave absorption. *Adv. Mater.* **2016**, *28*, 486–490. [CrossRef] [PubMed]

7. Yu, Q.; Chen, H.L.; Chen, P.; Wang, Q.; Lu, C.; Jia, C.X. Synthesis and electromagnetic absorption properties of $Fe_3O_4@C$ nanofibers/bismaleimide nanocomposites. *J. Mater. Sci. Mater. Electron.* **2017**, *28*, 2769–2774. [CrossRef]

8. Yu, Q.; Ma, M.; Chen, P.; Wang, Q.; Lu, C.; Gao, Y.; Wang, R.; Chen, H. Enhanced microwave absorption properties of electrospun PEK-C nanofibers loaded with Fe_3O_4/CNTs hybrid nanoparticles. *Eng. Sci.* **2017**, *57*, 1186–1192. [CrossRef]

9. Wen, B.; Cao, M.-S.; Lu, M.; Cao, W.; Shi, H.; Liu, J.; Wang, X.; Jin, H.; Fang, X.; Wang, W.; et al. Reduced Graphene Oxides: Light-Weight and High-Efficiency Electromagnetic Interference Shielding at Elevated Temperatures. *Adv. Mater.* **2014**, *26*, 3484–3489. [CrossRef]

10. Singh, A.P.; Mishra, M.; Hashim, D.P.; Narayanan, T.; Hahm, M.G.; Kumar, P.; Dwivedi, J.; Kedawat, G.; Gupta, A.; Singh, B.P.; et al. Probing the engineered sandwich network of vertically aligned carbon nanotube–reduced graphene oxide composites for high performance electromagnetic interference shielding applications. *Carbon* **2015**, *85*, 79–88. [CrossRef]

11. Wen, B.; Wang, X.X.; Cao, W.Q.; Shi, H.L.; Lu, M.M.; Wang, G.; Jin, H.B.; Wang, W.Z.; Yuan, J.; Cao, M.-S. Reduced graphene oxides: The thinnest and most lightweight materials with highly efficient microwave attenuation performances of the carbon world. *Nanoscale* **2014**, *6*, 5754–5761. [CrossRef] [PubMed]

12. Li, X.; Feng, J.; Du, Y.; Bai, J.; Fan, H.M.; Zhang, H.-L.; Peng, Y.; Li, F. One-pot synthesis of $CoFe_2O_4$/graphene oxide hybrids and their conversion into FeCo/graphene hybrids for lightweight and highly efficient microwave absorber. *J. Mater. Chem. A* **2015**, *3*, 5535–5546. [CrossRef]

13. Xu, W.; Wang, G.-S.; Yin, P.-G. Designed fabrication of reduced graphene oxides/Ni hybrids for effective electromagnetic absorption and shielding. *Carbon* **2018**, *139*, 759–767. [CrossRef]

14. Ye, W.; Fu, J.; Wang, Q.; Wang, C.; Xue, D. Electromagnetic wave absorption properties of NiCoP alloy nanoparticles decorated on reduced graphene oxide nanosheets. *J. Magn. Magn. Mater.* **2015**, *395*, 147–151. [CrossRef]

15. Zhang, S.L.; Jiao, Q.Z.; Hua, J.; Li, J.J.; Zhao, Y.; Li, H.S.; Wu, Q. Vapor diffusion synthesis of rugby-shaped $CoFe_2O_4$/graphene composites as absorbing materials. *J. Alloys Compd.* **2015**, *630*, 195–201. [CrossRef]

16. Chu, H.-R.; Zeng, Q.; Chen, P.; Yu, Q.; Xu, D.-W.; Xiong, X.-H.; Wang, Q. Synthesis and electromagnetic wave absorption properties of matrimony vine-like iron oxide/reduced graphene oxide prepared by a facile method. *J. Alloy Compd.* **2017**, *719*, 296–307. [CrossRef]

17. Yadav, R.S.; Kuřitka, I.; Vilčáková, J.; Machovský, M.; Škoda, D.; Urbánek, P.; Masař, M.; Gořalik, M.; Urbánek, M.; Kalina, L.; et al. Polypropylene Nanocomposite Filled with Spinel Ferrite $NiFe_2O_4$ Nanoparticles and In-Situ Thermally-Reduced Graphene Oxide for Electromagnetic Interference Shielding Application. *Nanomaterials* **2019**, *9*, 621. [CrossRef] [PubMed]

18. Mazzoli, A.; Corinaldesi, V.; Donnini, J.; Di Perna, C.; Micheli, D.; Vricella, A.; Pastore, R.; Bastianelli, L.; Moglie, F.; Primiani, V.M. Effect of graphene oxide and metallic fibers on the electromagnetic shielding effect of engineered cementitious composites. *J. Eng.* **2018**, *18*, 33–39. [CrossRef]

19. Qing, Y.C.; Min, D.D.; Zhou, Y.Y.; Luo, F.; Zhou, W.C. Graphene nanosheet-and flake carbonyl iron particle-filled epoxy-silicone composites asthin-thickness and wide-bandwidth microwave absorber. *Carbon* **2015**, *86*, 98–107. [CrossRef]

20. Micheli, D.; Pastore, R.; Vricella, A.; Marchetti, M. Matter's Electromagnetic Signature Reproduction by Graded-Dielectric Multilayer Assembly. *IEEE Trans. Microw. Theory Tech.* **2017**, *65*, 2801–2809. [CrossRef]

21. Micheli, D.; Pastore, R.; Delfini, A.; Giusti, A.; Vricella, A.; Tolochko, O.; Vasilyeva, E.; Santoni, F.; Marchetti, M. Electromagnetic characterization of advanced nanostructured materials and multilayer design optimization for metrological and low radar observability applications. *Acta Astronaut.* **2017**, *134*, 33–40. [CrossRef]

22. Xu, D.W.; Yang, S.; Chen, P.; Yu, Q.; Xiong, X.H.; Wang, J. Synthesis of magnetic graphene aerogels for microwave absorption by a in-situ pyrolysis. *Carbon* **2019**, *146*, 301–312. [CrossRef]

23. Zeng, Q.; Xiong, X.-H.; Chen, P.; Yu, Q.; Wang, Q.; Wang, R.-C.; Chu, H.-R. Air@rGO€Fe$_3$O$_4$ microspheres with spongy shells: Self-assembly and microwave absorption performance. *J. Mater. Chem. C* **2016**, *4*, 10518–10528. [CrossRef]

24. He, H.; Gao, C. Supraparamagnetic, Conductive, and Processable Multifunctional Graphene Nanosheets Coated with High-Density Fe$_3$O$_4$ Nanoparticles. *ACS Appl. Mater. Interfaces* **2010**, *2*, 3201–3210. [CrossRef] [PubMed]

25. He, J.-Z.; Wang, X.-X.; Zhang, Y.-L.; Cao, M.-S. Small magnetic nanoparticles decorating reduced graphene oxides to tune the electromagnetic attenuation capacity. *J. Mater. Chem. C* **2016**, *4*, 7130–7140. [CrossRef]

26. Zhang, M.; Liu, E.; Cao, T.; Wang, H.; Shi, C.; Li, J.; He, C.; He, F.; Ma, L.; Zhao, N. Sandwiched graphene inserted with graphene-encapsulated yolk–shell γ-Fe$_2$O$_3$ nanoparticles for efficient lithium ion storage. *J. Mater. Chem. A* **2017**, *5*, 7035–7042. [CrossRef]

27. Kou, L.; He, H.; Gao, C. Click chemistry approach to functionalize two-dimensional macromolecules of graphene oxide nanosheets. *Nano-Micro Lett.* **2010**, *2*, 177–183. [CrossRef]

28. Zhang, T.; Huang, D.; Yang, Y.; Kang, F.; Gu, J. Fe$_3$O$_4$/carbon composite nanofiber absorber with enhanced microwave absorption performance. *Mater. Sci. Eng. B* **2013**, *178*, 1–9. [CrossRef]

29. Hou, Z.L.; Zhang, M.; Kong, L.B.; Fang, H.M.; Li, Z.J.; Zhou, H.F.; Jin, H.B.; Cao, M.S. Microwave permittivity and permeability experiments in high-loss dielectrics: Caution with implicit Fabry-Perot resonance for negative imaginary permeability. *Appl. Phys. Lett.* **2013**, *103*, 162905. [CrossRef]

30. Wang, L.; Jia, X.; Li, Y.; Yang, F.; Zhang, L.; Liu, L.; Ren, X.; Yang, H. Sythesis and microwave absorption property of flexible magnetic film based on graphene oxide/carbon nanotubes and Fe$_3$O$_4$ nanoparticles. *J. Mater. Chem. A* **2014**, *2*, 14940–14946. [CrossRef]

31. Yang, H.; Ye, T.; Lin, Y.; Liu, M. Preparation and microwave absorption property of graphene/BaFe$_{12}$O$_{19}$/CoFe$_2$O$_4$ nanocomposite. *Appl. Surf. Sci.* **2015**, *357*, 1289–1293. [CrossRef]

32. Wang, Z.; Wu, L.; Zhou, J.; Jiang, Z.; Shen, B. Chemoselectivity-induced multiple interfaces in MWCNT/Fe$_3$O$_4$@ZnO heterotrimers for whole X-band microwave absorption. *Nanoscale* **2014**, *6*, 12298–12302. [CrossRef] [PubMed]